Cross Correlating Tidal Reconstructed 21cm Signal with Kinematic Sunyaev-Zel'dovich Effect: A New Probe for Missing Baryons at $z \sim 1-2$

Dongzi Li,[1,2] Ue-Li Pen,[3,4,5,1] Hong-Ming Zhu,[6,7] and Yu Yu[8]

[1]*Perimeter Institute for Theoretical Physics, 31 Caroline St. N., Waterloo, ON, N2L 2Y5, Canada*
[2]*University of Waterloo, 200 University Ave W, Waterloo, ON, N2L 3G1, Canada*
[3]*Canadian Institute for Theoretical Astrophysics, 60 St. George Street, Toronto, Ontario M5S 3H8, Canada*
[4]*Dunlap Institute for Astronomy and Astrophysics, 50 St. George Street, Toronto, Ontario M5S 3H4, Canada*
[5]*Canadian Institute for Advanced Research, CIFAR Program in Gravitation and Cosmology, Toronto, Ontario M5G 1Z8, Canada*
[6]*Key Laboratory for Computational Astrophysics, National Astronomical Observatories, Chinese Academy of Sciences, 20A Datun Road, Beijing 100012, China*
[7]*University of Chinese Academy of Sciences, Beijing 100049, China*
[8]*Key laboratory for research in galaxies and cosmology, Shanghai Astronomical Observatory, Chinese Academy of Sciences, 80 Nandan Road, Shanghai 200030, China*

(Dated: May 23, 2016)

The kinetic Sunyaev-Zel'dovich(kSZ) effect on Cosmic Microwave Background(CMB), induced by radial momentum of hot electrons, is a powerful tracer to probe baryon distributions. However, the signal is weak and lack of redshift information, hence another survey with spectroscopic redshift is typically required. This largely limits the sky area and depth to harness kSZ. Here, we propose a new source for cross correlation— HI density field from 21cm intensity mapping. 21cm spectra provide accurate redshift and intensity mappings integrate weak diffuse spectra, and thus can survey large sky area with great depth in much shorter time with low costs.

One main concern of the method is that the complicate 21cm foregrounds will contaminate radial large scale information, and reduce the correlation with kSZ. For redshift 1 and 2, we model the noise filtering in simulations, and find that after velocity reconstructions, there is $\gtrsim 0.7$ correlation with kSZ signal for $\ell \gtrsim 800$, and it drops for smaller ℓ. To improve the correlation for smaller ℓ, we recover large scale modes from their tidal influence on small scale structures (Cosmic Tidal Reconstruction). Successfully recover $> 90\%$ information at $k \sim 0.01h/Mpc$, we obtain a correlation $r \sim 0.6-0.8$ for $\ell \sim 100-2000$. The overall S/N for $\ell \sim 300-4000$ assuming Planck noise scale can reach 45 for $z = 1$, and 59 for $z = 2$. Since the reconstructed field and foreground filtered field are superior in different modes, it is easy to combine them and improve S/N for $\ell \sim 1000$.

PACS numbers:

I. INTRODUCTION

While the baryon abundance of early universe is well fixed [1–4], at $z \lesssim 2$ the detected baryon content in collapsed objects, eg. galaxies, galaxy clusters and groups, only accounts for 10% of the predicted amount. More baryons are believe to reside in Warm-Hot Intergalactic Mediums (WHIM) with typical temperature of 10^5 K to 10^7 K [5][6], which is too cold and diffuse to be detected. Continuous effort has been made to detect this part of baryons. One common approach is using hydrogen and metal absorption lines(eg, HI, Mg II,Si II, C II, Si III, C III, Si IV, O VI, O VII) [7][8]. However, the lines are usually limited to close circumgalactic medium, while at least 25% of the baryons are bebieved to reside in more diffused region [9]. Moreover, the uncertainty in metalicity would sometimes reduce the reliability.

A promising tool to probe the missing baryon is the kinetic Sunyaev-Zel'dovich(kSZ) effect [10][11], an effect that is greatly known for its potential to explore the Epoch of Reionization [12][13][14]. It refers to the secondary temperature anisotropy in CMB caused by Compton-scattering of CMB photon with free electrons. The radial velocity of electrons will give a Doppler shift to Since kSZ signal only relates to electron density and radial velocity, regardless the temperature and pressure, and velocity mainly results from large scale structure, the method is less biased towards hot, compact place, and provide more information on the fraction of diffused baryons.

Attractive as it is, due to the contamination of primary CMB, facility noises and probably residual thermal SZ signal, it is difficult to filter for the kSZ signal independently. Worse still, the signal itself does not contain redshift information.

To fix this, previous approches cross correlated it with galaxy surveys, eg. using pairwise-momentum estimator [15] or velocity-field-reconstruction estimator [16][17]. However since they all require spectroscopy of galaxies to provide accurate redshift, the sky volume and redshift range to apply the method is limited. A recent effort try to fix this using projected fields of galaxies, which is cheap and feasible [18]. However, projected fields only make use of information from the largest scale in z direction, while for $l \gtrsim 1000$, where primary CMB fades away, a sufficient amount of kSZ signal comes from smaller scales. This limits the accuracy and S/N it can reach.

In this paper we put forward a new tracer for cross correlation—HI density field from 21cm intensity mapping. Density contrast from 21cm spectra have accurate redshift information, which enables us to reconstruct velocity field and get better correlation with kSZ powerspectra. Moreover, intensity mapping is a kind of surveys that integrates different signals, rather than distinguishing individual galaxies. It accumulates contributions from weak sources and hence be able to reach high S/N at shorter time. There are already several ongoing 21cm experiments aim at large sky coverage and claim to be able to reach $z \gtrsim 1$ in very near future. CHIME [19], Tianlai [20], HIRAX [21] etc. Therefore, this correlator is

more feasible than large galaxy spectroscopic surveys, and more accurate that projected field.

However, the 21cm density field has its own drawback—the complicated foregrounds results from integration. While a cosmic signal in 21cm measurement is of the order of mK, foregrounds coming from Galactic emissions, telescope noise, extragalactic radio sources and Radio recombination lines, can reach the order of Kelvin [22][23]. Lots of techniques have been developed to substract the foregrounds, taking advantage of the attribute that they have fewer bright spectral degrees of freedom[24]. Unfortunately, substraction will contaminates the smooth large scale structure information in radial direction. Since the kSZ signal coming from a both density and velocity field, and velocity is greatly related to large scale structures. This drawback will inhibit the cross correlation behavior.

In this paper, we first discuss the influence of foregrounds and small scale noises, based on simulation and analysis. To improve the correlation, we for apply a new method called 3D Cosmic Tidal Reconstruction [25][26], which recover the large scale modes of density field from its tidal influence on small scale structures.

The paper is organized as follows: In section II, we demonstrate given a density field, how to correlate with kSZ signal with velocity reconstruction, similar to **??**; In section III, we present the result of cross correlation with foreground filtered field and discuss the behavior; Then in section IV, we introduce the method of 3D tidal reconstruction, and present the correlation results after small k modes recovered, In section V, we discuss redshift space distortions and estimate statistical errors, and we conclude at section VI.

Notes: Throughout the paper, We use the $z = 1, 2$ output of six N-body simulations from the CUBEP^{3}M code [27], each evolving 1024^3 particles in a $(1.2\mathrm{Gpc}/h)^3$ box. Simulation parameters are as follows: Hubble parameter $h = 0.678$, baryon density $\Omega_b = 0.049$, dark matter density $\Omega_c = 0.259$, amplitude of primordial curvature power spectrum $A_s = 2.139 \times 10^{-9}$ at $k_0 = 0.05\ \mathrm{Mpc}^{-1}$ and scalar spectral index $n_s = 0.968$.

we use "$\wedge$" to denote recontructed fields as oppose to fields directly from simulations.

II. VELOCITY RECONSTRUCTION AND KSZ SIGNALS CROSS CORRELATION

The CMB temperature fluctuations caused by kSZ effect is:

$$\Theta_{kSZ}(\hat{n}) \equiv \frac{\Delta T_{kSZ}}{T_{\mathrm{CMB}}} = -\frac{1}{c}\int d\eta g(\eta)\boldsymbol{p}_{\parallel}\ , \tag{1}$$

where $\eta(z)$ is the comoving distance at redshift z, $g(\eta) = e^{-\tau}d\tau/d\eta$ is the visibility function, τ is the optical depth to Thomson scattering, $\boldsymbol{p}_{\parallel} = (1+\delta)\boldsymbol{v}_{\parallel}$, with δ the electron overdensity. We assume that $g(\eta)$ doesn't change significally in one redshift bin, and integrate $\boldsymbol{p}_{\parallel}$ along radial axis to get $\hat{\Theta}_{kSZ}$

Due to the cancellation of positive and negative velocity, its direct cross correlation between kSZ signal will vanish. To better maintain the one to one multiplication between velocity field and density contrast, we first calculates the linear peculiar velocity, and then generate a mock kSZ signal [16]. In this way, we can at most maximize the correlation.

Assume we have a density contrast field $\delta = \frac{\rho-\bar{\rho}}{\bar{\rho}}$, where $\bar{\rho}$ is the average density of a certain redshift slice.

Detailed steps are as follows.

(1) Estimate the velocity field:

In linear region, the continuity equation goes like: $\dot{\delta} + \nabla \cdot \boldsymbol{v} = 0$, where $\boldsymbol{v}$ is the peculiar velocity and δ is the matter overdensity.

Therefore, we obtain an estimator of velocity distribution from the density contract δ:

$$\hat{v}_z(\boldsymbol{k}) = iaHf\delta(\boldsymbol{k})\frac{k_z}{k^2} \tag{2}$$

where $f = \frac{d\ln D}{d\ln a}$, D(a) is the linear growth function, a is the scale factor, H is the Hubble parameter.

$v_z \propto \frac{k_z}{k^2}$, indicating the most prominent signal comes from small k mode, which corresponds to large scale structure.

(2) suppress the noise in velocity field with a Wiener filter. This is because the term $\frac{k_z}{k^2}$ in Eq.(2) will strongly amplify noises in small k modes.

$$\hat{v}_z^c(\boldsymbol{k}) = \frac{\hat{v}_z(\boldsymbol{k})}{b(k_\perp, k_\parallel)}W(k_\perp, k_\parallel)\ , \tag{3}$$

Bias $b = \frac{P_{\hat{v}_z, v_z}}{P_{v_z}}$, Wiener filter $W = \frac{P_{v_z}}{P_{\hat{v}_z}/b^2}$.

(3) Calculate 2D kSZ map follow Eq.(1).

(4) Calculate correlation coefficients.

We compare reconstructed kSZ signals $\hat{\Theta}_{kSZ}$ with kSZ signals Θ_{kSZ} directly from simulations. To quantify the tightness of correlation, we employ a quantity r:

$$r \equiv \frac{P_{recon,real}}{\sqrt{P_{recon}P_{real}}} \tag{4}$$

III. CROSS CORRELATION WITH NOISE SUBSTRACTED FIELD

A. Mimic the Noise Substraction

To ressemble realistic observations, we take into account the resolution, small scale noises and foreground substractions. Two filters are applied on original density contrast δ to imitate the effects of noise substractions:

1. For small scale noises:

Import a cut off scale k_c with a step function $H(k_c - k)$. For $k > k_c$, $H(k_c - k) = 0$; for $k \leqslant k_x$; $H(k_c - k) = 1$. This is reasonable for a filled aperture experiment, which has good brightness sensitivity and an exponetially growing noise at small scales. We choose $k_c = 0.5\ h/\mathrm{Mpc}$ and $0.32h/\mathrm{Mpc}$ respectively for $z = 1$ and $z = 2$, which corresponds to $\ell \sim 1150$. This is generally realistic, judging from ongoing 21cm experiments like CHIME [19][28] and Tianlai [29][20].

2. For foreground noises:

Use a high pass filter $W_{fs}(k_\parallel) = 1 - e^{-k_\parallel^2 R_\parallel^2/2}$ to imitate the substraction. We choose $R_\parallel = 15\ \mathrm{Mpc}/h$ for $z = 1$

and $R_\parallel = 8\ \mathrm{Mpc}/h$ for $z = 2$, which gives $W_{fs} = 0.5$ at $k_\parallel = 0.08\ \mathrm{Mpc}/h$ and $0.15\ \mathrm{Mpc}/h$ respectively.

The observed 21cm field after noises subtraction is then given by

$$\delta_{ns}(\boldsymbol{k}) = \delta(\boldsymbol{k}) W_{fs}(k_\parallel) J(k_c - k), \tag{5}$$

With the noise filtered density contrast δ_{ns}, we follow the procedure described in last section to generate a mock kSZ signal $\hat{\Theta}_{ns}$ and calculate cross correlation $r_{\Theta\hat{\Theta}_{ns}}$.

B. Cross Correlation from Noise Substracted Field

Fig.1 upper panel Shows the cross correlation between the reconstructed velocity field $\hat{v}_{z,ns}$ and the real velocity field v_z, at redshift 1 and 2.

At this point, all the manipulation and calculation on $\delta(\boldsymbol{k})$ are independent over different $\boldsymbol{k}$, therefore, the cross-correlation closely resembles the substraction we perform.

Just one interesting thing to notice is that although the foreground at z=2 is stronger, the non-linear effects are weaker. So we still can obtain correlations at $k_\parallel \lesssim 0.1$ with the seriously suppressed density contrast.

Fig.2 shows the cross correlation between the reconstructed kSZ map $\hat{\Theta}_{ns}$ and real kSZ map Θ at redshift 1 and 2.

There are two points to notice:

(1) For both redshift, there are a considerable amount of correlation $r \gtrsim 0.5$ for $l \gtrsim 1000$; and this correlation drops quickly for smallerℓ;

(2) The obtained correlation at redshift 2 is better than redshift 1.

Although not satisfactory at smallℓ, the reconstructed kSZ signal $\hat{\Theta}_{ns}$ from 21cm density field shall already be able to give us reasonable S/N in real applications , because most kSZ signals that can actually be distinguished come from at least $l \gtrsim 500$, when primary CMB gradually dies out.

C. Explanation of the Cross Correlation Behavior

To explain the behavior of the cross correlation, we write Eq.(1) in Fourier space.

$$\Theta(\tilde{\boldsymbol{k}}_\perp) \equiv \ \Theta\ (\tilde{k}_x, \tilde{k}_y, 0) \propto \int d^3k \delta(\tilde{\boldsymbol{k}}_\perp - \boldsymbol{k}_\perp, k_\parallel) v_z(\boldsymbol{k})$$
$$\xrightarrow[region]{linear} \int d^3k \delta(\tilde{\boldsymbol{k}}_\perp - \boldsymbol{k}_\perp, k_\parallel) \delta(\boldsymbol{k}) \frac{k_z}{k^2} \tag{6}$$

$$\langle \Theta(\tilde{\boldsymbol{k}}_\perp) \Theta^*(\tilde{\boldsymbol{k}}_\perp) \rangle \ \propto \int \frac{d^3\boldsymbol{k}}{(2\pi)^3} \frac{d^3\boldsymbol{k'}}{(2\pi)^3} \frac{k_z}{k^2} \frac{k'_z}{k'^2} \tag{7}$$
$$\langle \delta(\boldsymbol{k}) \delta(\tilde{\boldsymbol{k}}_\perp - \boldsymbol{k}) \delta^*(\boldsymbol{k'}) \delta^*(\tilde{\boldsymbol{k}}_\perp - \boldsymbol{k'}) \rangle$$

The dominate term is $\langle \delta(\boldsymbol{k}) \delta^*(\boldsymbol{k'}) \rangle \langle \delta(\tilde{\boldsymbol{k}}_\perp - \boldsymbol{k}) \delta^*(\tilde{\boldsymbol{k}}_\perp - \boldsymbol{k'}) \rangle$

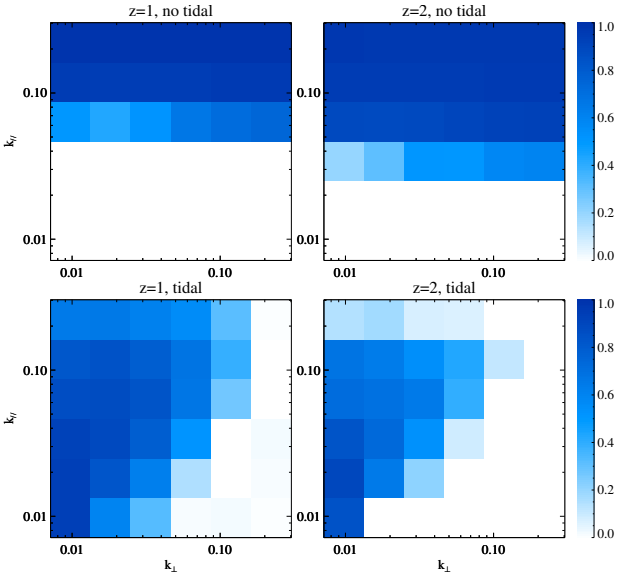

FIG. 1: (Top) The cross correlation r between P_{v_z} and $P_{\hat{v}_z^{fs}}$ calculated from foreground filtered field δ_{fs}; (Bottom) The cross correlation between P_{v_z} and $P_{\hat{v}_z^{tide}}$ calculated from $\hat{\kappa}_c$.

and $\langle \delta(\boldsymbol{k}) \delta^*(\tilde{\boldsymbol{k}}_\perp - \boldsymbol{k'}) \rangle \langle \delta(\tilde{\boldsymbol{k}}_\perp - \boldsymbol{k}) \delta^*(\boldsymbol{k'}) \rangle$, hence,

$$\langle \Theta(\tilde{\boldsymbol{k}}_\perp) \Theta^*(\tilde{\boldsymbol{k}}_\perp) \rangle \propto \int d^3\boldsymbol{k} d^3\boldsymbol{k'} \frac{k_z}{k^2} \frac{k'_z}{k'^2} \tag{8}$$
$$P(k) P(\tilde{\boldsymbol{k}}_\perp - \boldsymbol{k}) [\delta^D(\boldsymbol{k} - \boldsymbol{k'}) + \delta^D(\boldsymbol{k} + \boldsymbol{k'} - \tilde{\boldsymbol{k}}_\perp)]$$
$$= \int d^3 \ln \boldsymbol{k} \frac{k_z^3 k_x k_y}{k^2} P(k) P(\tilde{\boldsymbol{k}}_\perp - \boldsymbol{k}) (\frac{1}{k^2} - \frac{1}{|\tilde{\boldsymbol{k}}_\perp - \boldsymbol{k}|^2})$$

We transform $dk \to d \ln k$ to show the contributions from different k scales. Level of $P(k)$ can be seen in Fig.**??**

For small $\tilde{k}'_\perp \sim 0.01$ h/Mpc, which corresponds to $\ell \sim 20 - 30$:

Most $(\frac{1}{k^2} - \frac{1}{|\tilde{\boldsymbol{k}}_\perp - \boldsymbol{k}|^2}) \sim \frac{1}{k^3}$, so we have $\frac{k_z^3 k_x k_y}{k^5}$ which is scale invariant , and $P(k)\, P(\tilde{\boldsymbol{k}}_\perp - \boldsymbol{k})$ reach peak at similar point with small k. Therefore, main contribution of the powerspectrum is from large scale. On the other hand, the fields after foreground substraction lack the part from small k, which causes the null correlation.

For large $\tilde{k}'_\perp \sim$ 1h/Mpc:
$(\frac{1}{k^2} - \frac{1}{|\tilde{\boldsymbol{k}}_\perp - \boldsymbol{k}|^2}) \sim \frac{1}{k^2}$ or even $\sim \frac{1}{\tilde{k}_\perp^2}$ so we have at least $\frac{k_z^3 k_x k_y}{k^4}$, which prefers small scales. Moreover, $P(k)\, P(\tilde{\boldsymbol{k}}_\perp - \boldsymbol{k})$ no longer reach peak at similar point. Therefore, the importance of small k modes is attenuated, and the influence of foregrounds are reduced.

The reason why the correlation on redshift 2 is better is that the density contrast at redshift 1 is sharper than redshift 2, which exaggerates the contribution from small scales.

IV. 3D COSMIC TIDAL RECONSTRUCTION

Since the loss of large scale information in z direction will reduce the cross correlation with small ℓ and influence the

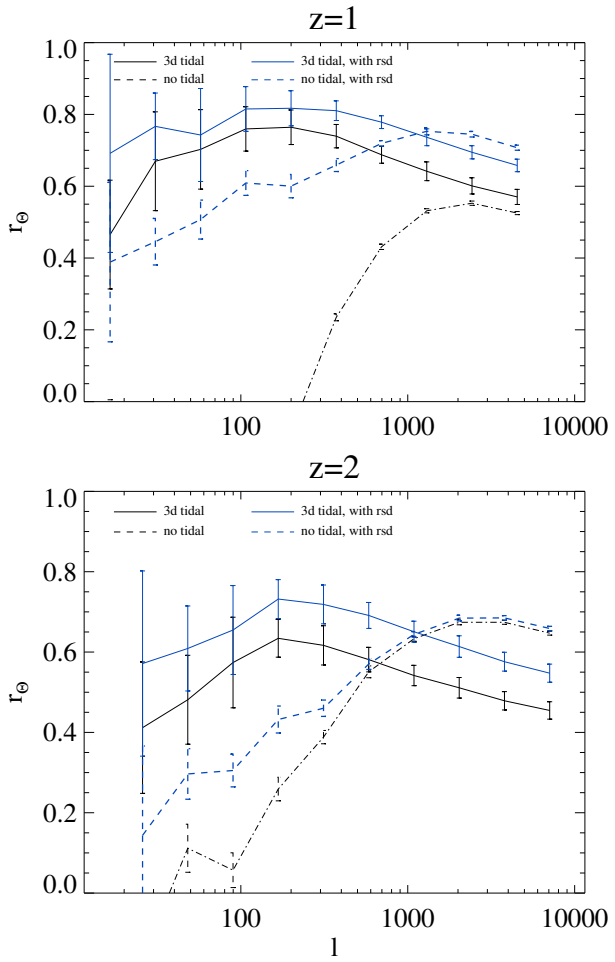

FIG. 2: The cross correlation r between reconstructed kSZ $P_{\hat{\Theta}_{kSZ}}$ and real kSZ $P_{\Theta_{kSZ}}$. (Dashed line) kSZ calculated from foreground filtered 21cm density field δ_{fs}; (Solid line) kSZ calculated from tidal reconstructed density field.

performance on large ℓ. We try to recover the modes with a method called Cosmic Tidal Reconstruction. This is one of the first application of its 3D version.

A. Algorithm

The fundamental idea of Cosmic Tidal Reconstruction is that the evolution of small scale structure is modulated by large scale gravitational force. We can select this effect and solve for the large scale potential.

Main Procedure:

Consider only the anisotropic influence from tidal force, the distortions on power spectrum [26] can linearly be calculated as

$$\delta P(\boldsymbol{k},\tau)|_{t_{ij}} = \hat{k}^i\hat{k}^j t_{ij}^{(0)} P_{1s}(k,\tau) f(k,\tau) \tag{9}$$

where f is the linear coupling function; $P_{1s}(k,\tau)$ is the theoretical small scale linear powerspectrum; and $\delta P(\boldsymbol{k},\tau)$ is the real distortion from observations.

Hence we can solve for the unknown quantity t_{ij}, which is the tidal force tensor defined as

$$t_{ij} = \Phi_{L,ij} - \nabla^2\Phi_L \delta^D_{ij}/3 \tag{10}$$

$\Phi_{L,ij}$ is the second derivative of large scale potential, δ^D is the Dirac function.

With t_{ij}, we calculate the variance of large scale potential Φ_L and get the large scale density contrast κ_{3D}.

$$\kappa_{3D} \sim \nabla^2\Phi_L = \frac{3}{2}\frac{\partial_i\partial_j}{\nabla^2} t_{ij} \tag{11}$$

Since $f(k,\tau)$ increase with k in our interested scales, the distortions are more obvious in small scales. Therefore, the method mainly use the quadratic statistics on small scales to recover the large scale density field. It works best for close linear regions.

Detailed steps:

(1) Gaussianize the field, taking $\delta_g = \ln(1+\delta)$. This is to allieviate the problem that filter W_i in Eq.(14) heavily weights high density regions.

(2) Following gravitational lensing procedures, decompose the symmetric, traceless tidal force tensor into 5 components,

$$t_{ij} = \begin{pmatrix} \gamma_1 - \gamma_z & \gamma_\times & \gamma_2 \\ \gamma_\times & -\gamma_1 - \gamma_z & \gamma_y \\ \gamma_2 & \gamma_y & 2\gamma_z \end{pmatrix}. \tag{12}$$

(3) Select density distortions caused by tidal force, by convolving δ_g with a filter W_i deduced from Eq.(9)

$$\delta_g^{w_i}(\boldsymbol{k}) = W_i(\boldsymbol{k})\delta_g(\boldsymbol{k}) \tag{13}$$

$$W_i(\boldsymbol{k}) = i(\frac{P(k)f(k)}{P^2_{tot}(k)})^{\frac{1}{2}}\frac{k_i}{k} = S(k)\frac{k_i}{k}$$

where i indicates $\hat{x},\hat{y},\hat{z}$ directions, $f(k) = 2\alpha(\tau) - \beta(\tau) d\ln P/d\ln k$ is again the coupling function, with α and β related to linear growth funcion [26], and calculated to be (0.6, 1.3) for $z=1$ and (0.4, 0.9) for $z=2$. $P_{tot} = P + P_{noise}$ is observed matter powerspectrum, P is theoretical matter powerspectrum,

(4) Estimate the 5 tidal tensor components from quadratic statistics.

$$\begin{aligned}
\hat{\gamma}_1(\boldsymbol{x}) &= [\delta_g^{w_1}(\boldsymbol{x})\delta_g^{w_1}(\boldsymbol{x}) - \delta_g^{w_2}(\boldsymbol{x})\delta_g^{w_2}(\boldsymbol{x})], \\
\hat{\gamma}_2(\boldsymbol{x}) &= [2\delta_g^{w_1}(\boldsymbol{x})\delta_g^{w_2}(\boldsymbol{x})], \\
\hat{\gamma}_x(\boldsymbol{x}) &= [2\delta_g^{w_1}(\boldsymbol{x})\delta_g^{w_3}(\boldsymbol{x})], \\
\hat{\gamma}_y(\boldsymbol{x}) &= [2\delta_g^{w_2}(\boldsymbol{x})\delta_g^{w_3}(\boldsymbol{x})], \\
\hat{\gamma}_z(\boldsymbol{x}) &= [(2\delta_g^{w_3}(\boldsymbol{x})\delta_g^{w_3}(\boldsymbol{x}) - \delta_g^{w_1}(\boldsymbol{x})\delta_g^{w_1}(\boldsymbol{x}) - \delta_g^{w_2}(\boldsymbol{x})\delta_g^{w_2}(\boldsymbol{x}))]/3,
\end{aligned} \tag{14}$$

(5) Reconstruct large scale density contrast κ_{3D} from tidal tensor:

$$\begin{aligned}
\kappa_{3D}(\boldsymbol{k}) = \frac{1}{k^2} \quad & [(k_1^2 - k_2^2)\gamma_1(\boldsymbol{k}) + 2k_1k_2\gamma_2(\boldsymbol{k}) \\
& +2k_1k_3\gamma_x(\boldsymbol{k}) + 2k_2k_3\gamma_y(\boldsymbol{k}) \\
& +(2k_3^2 - k_1^2 - k_1^2)\gamma_z(\boldsymbol{k})].
\end{aligned} \tag{15}$$

(6) Correct bias and suppress noise with a Wiener filter.

Due to the foregrounds, the noise in z direction will be different from x,y direction, therefore we apply an anisotropic Wiener filter.

$$\hat{\kappa}_c(\boldsymbol{k}) = \frac{\kappa_{3\rm D}(\boldsymbol{k})}{b(k_\perp, k_\parallel)} W(k_\perp, k_\parallel)\ , \tag{16}$$

Bias $b(k_\perp, k_\parallel) = \frac{P_{\rm k3D,\delta}}{P_\delta}$ is the cross powerspectra between reconstructed field κ3D and original field δ, Wiener filter $W(k_\perp, k_\parallel) = \frac{P_\delta}{P_{\rm k3D}/b^2}$.

Here $\hat{\kappa}_c$ is the output large scale density contrast we obtain from tidal reconstruction. We use it to calculate velocity $\hat{v}_z^{\rm tide}$ and mock kSZ signal $\hat{\Theta}_{\rm tide}$ following identical procedure as to noise filtered field.

B. Cross Correlation from Tidal Reconstructed Field

For comparison, we first present the cross correlation between v_z and $\hat{v}_z^{tide}$ in lower panels of Fig.1.

It is obvious that the previously lost small $k_\parallel$ modes are partly recovered. The reconstruction on $k_\parallel$ direction is better than on $k_\perp$ direction. This is because tidal reconstruction relies heavily on large k modes, yet lots of large $k_\perp$ modes, whose $k_\parallel$ is small, are lost in the foregrounds. There is degrading performance of tidal reconstruction on z=2 compared to z=1, which mainly results from the stricter cutoff $k_c = 0.32h/Mpc$ compared to $k_c = 0.5h/Mpc$.

In Fig.2, we demonstrate the correlation r between the reconstructed kSZ signal $\hat{\Theta}_{tide}$ and original kSZ signal Θ.

It is important to see: For z=1, there are significant improvement on the cross-correlation after tidal reconstruction, especially below $l \sim 2000$; for z=2, the cross-correlation is improved for $l \lesssim 800$. Combining noise filtered fields and tidal reconstructed fields, we shall have good cross-correlation for $l \sim 50 - 5000$, with the assumed level of foregrounds and noises on small scales.

C. Improvements on Reconstruction Procedure

Previously we go through standard tidal reconstruction procedure. However, since our noises are strongly denpendent on direction and scale, there are several steps that can help obtain more accurate reconstruction.

First, for Eq.14, there is a $P_{\rm tot} = P + P_{\rm noise}$ in the denominator of the filter W_i. Previously, we simply use P instead of $P_{\rm tot}$. A more accurate way to select relavant distortions has to consider different noise level of different scales. We can estimate the noise spectra following similar procedure as Eq.16, $P_{\rm noise}(k_\perp, k_\parallel) = P_{\delta_n s}(k_\perp, k_\parallel) - b^2(k_\perp, k_\parallel) P_\delta(k_\perp, k_\parallel)$ After that, we apply different renormalization to γs in eq.14. The effect is heavier weights assigned to large z, where cleanest signals come from.

Second, since different γ use different modes, their noise and bias are different. It is better to filter them seperately before combining together. Follow Eq.11, we could estimate the expected value of γ with $t_{ij} \sim \delta \frac{2}{3} \frac{k^2}{k_i k_j}$, where δ is the original field which has complete large scale structure. After that, we apply Wiener filter similar to Eq.16 to independent γ before getting κ.

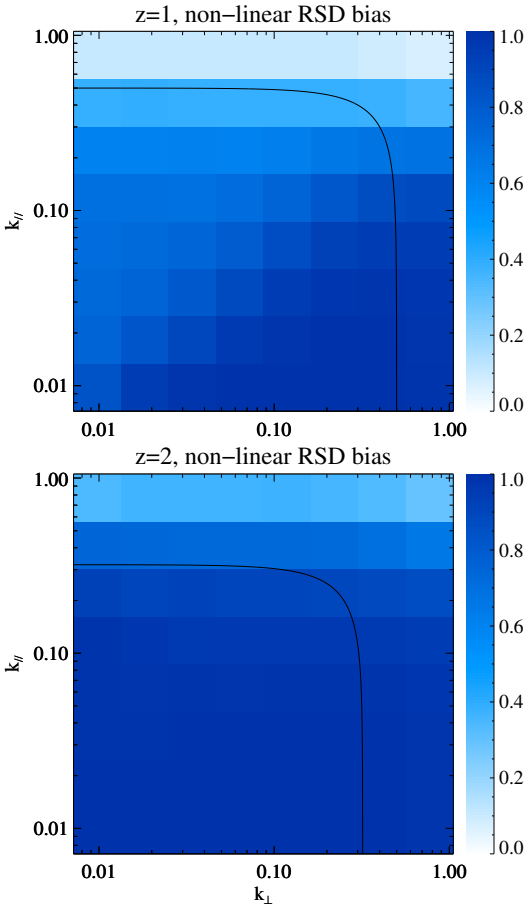

FIG. 3: The bias $b = P_{\delta_{\rm nlRSD},\delta}/P_\delta$ of redshift space distorted(RSD) field after linear RSD substraction.

V. DISCUSSION AND ERROR ESTIMATES

A. Redshift Distortion

The redshift space distortion(RSD) refers to the misjudgement on comoving distance results from peculiar velocity of objects. In this section we add the RSD effect to our original fields and study its influence on our reconstruction.

Linearly, RSD induces an additional contraction in z direction $\delta^{RSD}(\boldsymbol{k}) = (1 + f\mu^2)\delta(\boldsymbol{k})$. where $\mu = \frac{k_\parallel}{k}$. We can easily filter it by dividing the observed density contrast with $1 + f\mu^2$. However, for low redshift, non-linear effect may also play a role. Substracting the linear RSD, we present the bias between the remaining RSD field and field in real space $b = P_{\delta_{\rm nlRSD},\delta}/P_\delta$ in Fig.3. The dark line indicates

For z=2, until the cut off scale $k_c = 0.32$ h/Mpc the non-linear effect is still not very strong. However, for z=1, there are sufficient non-linear effects below $k_c = 0.5$ h/Mpc. Cannot

directly substract it, we go through identical procedures on redshift distorted fields, and see how much influence it exerts on cross correlation. The result is presented in Fig.2.

Much to our surprise, the cross correlation is even improved by 0.1. This is possibly because both RSD and foregrounds are in z direction. The contraction induced by RSD assigns more weigh to large k_z modes, and these are the most clean signals survived from foregrounds. Moreover, RSD assigns more weigh to shear estimators related to covariance in z directions, and this is where best tidal recovered modes come from. Hence, the field with RSD accidentally give us better results on cross correlation.

This is not the only advantage RSD brings. Actually the inhancement in large k_z will increase the S/N at that level, raise the cut off scale k_c and ultimately improve the reconstruction results. In all, redshift space distortion seems to be a blessing rather than problem in our case.

B. Statistical Error

We use the statistical error to estimate the S/N ratio for real surveys, taking into account the contamination from primary CMB and facility noises.

$$\frac{S}{N} = \frac{C_l}{\Delta C_l} \simeq r\sqrt{(2l+1)\Delta l f_{\rm sky}}\sqrt{\frac{C_l^{\rm kSZ,\Delta z}}{C_l^{\rm CMB}+C_l^{\rm kSZ}+C_l^{\rm CMB,N}}} \quad (17)$$

Where $C_l^{\rm CMB}$ is the angular powerspectrum of primary CMB; $C_l^{\rm CMB,N}$ indicates the facility noises; $C_l^{\rm kSZ,\Delta z}$ is the kSZ signal from a certain redshift bin; r is the correlation coefficients we get; $f_{\rm sky}$ is the percent of sky area covered by both surveys.

In our case, we calculate C_l^{CMB} from CAMB [30]. We use Planck 2015 results [31] at 217GHz to estimate $C_l^{CMB,N}$. $C_l^{\rm CMB,N} = (\sigma_{p,T}\theta_{\rm FWHM})^2 W_l^{-2}$; where $\sigma_{p,T} = 8.7\mu K_{\rm CMB}$ is Sensitivity per beam solid angle, $\theta_{\rm FWHM} \sim 5'$ is the effective beam FWHM, $W_l = \exp[-l(l+1)/2l_{\rm beam}^2]$ is the smoothing window function, with $l_{\rm beam} = \sqrt{8\ln 2}/\theta_{\rm FWHM}$. We choose $f_{\rm sky} = 0.8$, since it is feasible for 21cm intensity mapping to survey large sky areas. We choose $\Delta l/l = 0.1$. And for $C_l^{\rm kSZ,\Delta z}$, we choose two bins of size 1200 Mpc/h, centered at redshift 1,2 respectively.

In Fig.4, we plot the S/N level for the two redshift bins. The S/N will exceeds 3 from $l \sim 500 - 3000$. The overall S/N for $z \approx 1$ is 45, and for $z \approx 2$ is 59.

Since we only use the correlation calculated from tidal reconstructed field, the S/N shall be higher for z=2 combining tidal reconstructed field and foreground filtered field. Moreover, since C_l^{kSZ} is relatively flat, it is possible to bin it into larger Δl.

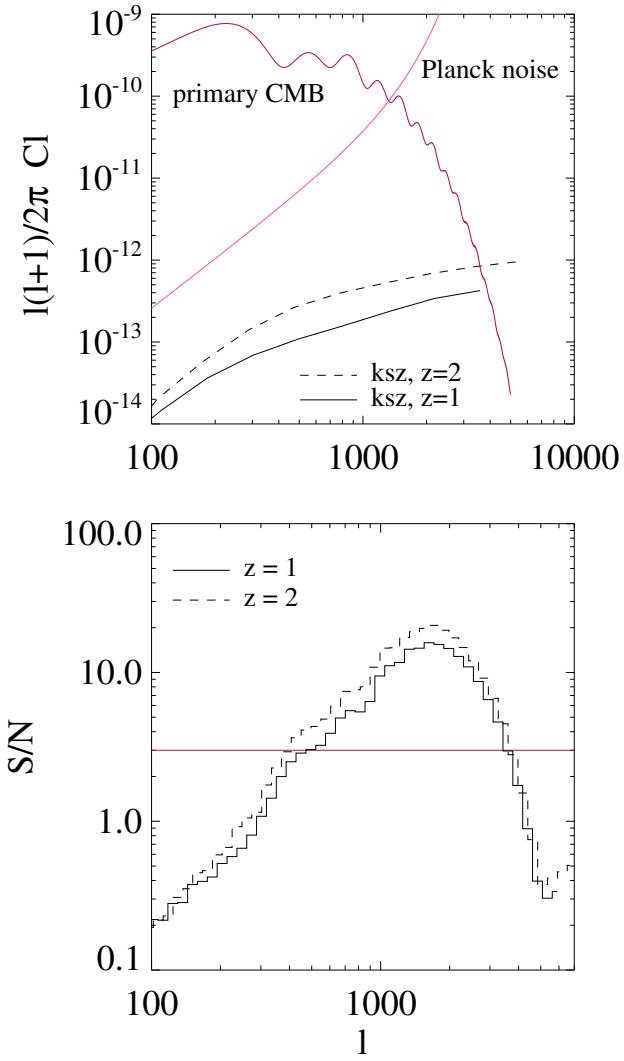

FIG. 4: (Top) Relative strength of kSZ signal, within a box of $\Delta\chi = 1200 Mpc/h$. (Bottom) predicted S/N, assuming Planck noise, $\Delta l/l = 0.1$, $f_{sky} = 0.8$.

VI. CONCLUSION

In this paper, we discuss the possibility of cross correlating kSZ signal with 21cm intensity mapping as a new probe to study baryon distributions. A tomographic way of calculating cross correlation with estimated velocity field is applied. Correlation results are presented for redshift 1 and 2, considering foreground noises, finite telescope resolution, and redshift space distortions. The latter two will not matter much. However, the foreground noise will smear the correlation on large scales while leaving sufficient correlation on smaller scales such as $\ell \sim 1000$. In order to study the large scale baryon distribution, we recover modes lost in foregrounds with a 3D tidal reconstruction and obtain a $r > 0.6$ correlation for $\ell \sim 100 - 2000$. After the reconstruction, we will likely be able to distinguish cross correlation signals from $\ell \gtrsim 500$. Assuming Planch noise, the total S/N can reach 45 for $z = 1$ and

59 for $z = 2$. This shows a promising future for this method.

VII. ACKNOWLEDGE

We acknowledge discussions with Kendrick Smith, Matthew Johnson, Wenkai Hu, Tianxiang Mao and Jiawei Shao. The simulations were performed on the BGQ supercomputer at the SciNet HPC Consortium. SciNet is funded by: the Canada Foundation for Innovation under the auspices of Compute Canada; the Government of Ontario; the Ontario Research Fund – Research Excellence; and the University of Toronto. Research at the Perimeter Institute is supported by the Government of Canada through Industry Canada and by the Province of Ontario through the Ministry of Research & Innovation. The Dunlap Institute is funded through an endowment established by the David Dunlap family and the University of Toronto.

[1] R. J. Cooke, M. Pettini, R. A. Jorgenson, M. T. Murphy, and C. C. Steidel, ApJ **781**, 31 (2014), 1308.3240.
[2] G. Hinshaw, D. Larson, E. Komatsu, D. N. Spergel, C. L. Bennett, J. Dunkley, M. R. Nolta, M. Halpern, R. S. Hill, N. Odegard, et al., ApJS **208**, 19 (2013), 1212.5226.
[3] E. Komatsu, K. M. Smith, J. Dunkley, C. L. Bennett, B. Gold, G. Hinshaw, N. Jarosik, D. Larson, M. R. Nolta, L. Page, et al., ApJS **192**, 18 (2011), 1001.4538.
[4] G. Hinshaw, D. Larson, E. Komatsu, D. N. Spergel, C. L. Bennett, J. Dunkley, M. R. Nolta, M. Halpern, R. S. Hill, N. Odegard, et al., ApJS **208**, 19 (2013), 1212.5226.
[5] U.-L. Pen, ApJ **510**, L1 (1999), astro-ph/9811045.
[6] A. M. Sołtan, A&A **460**, 59 (2006), astro-ph/0604465.
[7] M. Fukugita and P. J. E. Peebles, ApJ **616**, 643 (2004), astro-ph/0406095.
[8] J. K. Werk, J. X. Prochaska, J. Tumlinson, M. S. Peeples, T. M. Tripp, A. J. Fox, N. Lehner, C. Thom, J. M. O'Meara, A. B. Ford, et al., ApJ **792**, 8 (2014), 1403.0947.
[9] R. Davé, B. D. Oppenheimer, N. Katz, J. A. Kollmeier, and D. H. Weinberg, MNRAS **408**, 2051 (2010), 1005.2421.
[10] R. A. Sunyaev and Y. B. Zeldovich, Comments on Astrophysics and Space Physics **4**, 173 (1972).
[11] R. A. Sunyaev and I. B. Zeldovich, MNRAS **190**, 413 (1980).
[12] P. Zhang, U.-L. Pen, and H. Trac, MNRAS **347**, 1224 (2004), astro-ph/0304534.
[13] M. McQuinn, S. R. Furlanetto, L. Hernquist, O. Zahn, and M. Zaldarriaga, ApJ **630**, 643 (2005), astro-ph/0504189.
[14] O. Zahn, C. L. Reichardt, L. Shaw, A. Lidz, K. A. Aird, B. A. Benson, L. E. Bleem, J. E. Carlstrom, C. L. Chang, H. M. Cho, et al., ApJ **756**, 65 (2012), 1111.6386.
[15] N. Hand, G. E. Addison, E. Aubourg, N. Battaglia, E. S. Battistelli, D. Bizyaev, J. R. Bond, H. Brewington, J. Brinkmann, B. R. Brown, et al., Physical Review Letters **109**, 041101 (2012), 1203.4219.
[16] J. Shao, P. Zhang, W. Lin, Y. Jing, and J. Pan, MNRAS **413**, 628 (2011), 1004.1301.
[17] M. Li, R. E. Angulo, S. D. M. White, and J. Jasche, MNRAS **443**, 2311 (2014), 1404.0007.
[18] J. C. Hill, S. Ferraro, N. Battaglia, J. Liu, and D. N. Spergel, ArXiv e-prints (2016), 1603.01608.
[19] K. Bandura, G. E. Addison, M. Amiri, J. R. Bond, D. Campbell-Wilson, L. Connor, J.-F. Cliche, G. Davis, M. Deng, N. Denman, et al., in *Society of Photo-Optical Instrumentation Engineers (SPIE) Conference Series* (2014), vol. 9145 of *Society of Photo-Optical Instrumentation Engineers (SPIE) Conference Series*, p. 22, 1406.2288.
[20] Y. Xu, X. Wang, and X. Chen, ApJ **798**, 40 (2015), 1410.7794.
[21] http://www.acru.ukzn.ac.za/ hirax/.
[22] T. Di Matteo, B. Ciardi, and F. Miniati, MNRAS **355**, 1053 (2004), astro-ph/0402322.
[23] K. W. Masui, E. R. Switzer, N. Banavar, K. Bandura, C. Blake, L.-M. Calin, T.-C. Chang, X. Chen, Y.-C. Li, Y.-W. Liao, et al., ApJ **763**, L20 (2013), 1208.0331.
[24] E. R. Switzer, T.-C. Chang, K. W. Masui, U.-L. Pen, and T. C. Voytek, ApJ **815**, 51 (2015), 1504.07527.
[25] U.-L. Pen, R. Sheth, J. Harnois-Deraps, X. Chen, and Z. Li, ArXiv e-prints (2012), 1202.5804.
[26] H.-M. Zhu, U.-L. Pen, Y. Yu, X. Er, and X. Chen, ArXiv e-prints (2015), 1511.04680.
[27] J. Harnois-Déraps, U.-L. Pen, I. T. Iliev, H. Merz, J. D. Emberson, and V. Desjacques, MNRAS **436**, 540 (2013), 1208.5098.
[28] L. B. Newburgh, G. E. Addison, M. Amiri, K. Bandura, J. R. Bond, L. Connor, J.-F. Cliche, G. Davis, M. Deng, N. Denman, et al., in *Society of Photo-Optical Instrumentation Engineers (SPIE) Conference Series* (2014), vol. 9145 of *Society of Photo-Optical Instrumentation Engineers (SPIE) Conference Series*, p. 91454V, 1406.2267.
[29] X. Chen, International Journal of Modern Physics Conference Series **12**, 256 (2012), 1212.6278.
[30] A. Lewis, A. Challinor, and A. Lasenby, Astrophys. J. **538**, 473 (2000), astro-ph/9911177.
[31] Planck Collaboration, R. Adam, P. A. R. Ade, N. Aghanim, M. Arnaud, M. Ashdown, J. Aumont, C. Baccigalupi, A. J. Banday, R. B. Barreiro, et al., ArXiv e-prints (2015), 1502.01587.